# Clean quartz matters for cosmogenic nuclide analyses: an exploration of the importance of sample purity using the CRONUS-N reference material

For submission to Quaternary Geochronology

Lee B. Corbett<sup>1\*</sup>
Paul R. Bierman<sup>1</sup>
Thomas A. Brown<sup>2</sup>
Marc W. Caffee<sup>3,4</sup>
David Fink<sup>5</sup>
Stewart P.H.T. Freeman<sup>6</sup>
Alan J. Hidy<sup>2</sup>
Dylan H. Rood<sup>7</sup>
Klaus M. Wilcken<sup>5</sup>
Thomas E. Woodruff<sup>3</sup>

<sup>&</sup>lt;sup>1</sup> Rubenstein School for Environment and Natural Resources, University of Vermont, Burlington, Vermont, USA

<sup>&</sup>lt;sup>2</sup> Center for Accelerator Mass Spectrometry, Lawrence Livermore National Laboratory, Livermore, California, USA

<sup>&</sup>lt;sup>3</sup> Department of Physics and Astronomy, Purdue University, West Lafayette, Indiana, USA

<sup>&</sup>lt;sup>4</sup> Department of Earth, Atmospheric, and Planetary Sciences, Purdue University, West Lafayette, Indiana, USA

<sup>&</sup>lt;sup>5</sup> Australian Nuclear Science and Technology Organization, Lucas Heights, New South Wales, Australia

<sup>&</sup>lt;sup>6</sup> Scottish Universities Environmental Research Centre, East Kilbride, UK

<sup>&</sup>lt;sup>7</sup> Department of Earth Science and Engineering, Imperial College London, South Kensington Campus, London, UK

<sup>\*</sup> Contact author: Ashley.Corbett@uvm.edu

#### Abstract

1

20

2 Reference materials are key for assessing inter-laboratory variability and measurement quality, 3 and for placing analytical uncertainty bounds on sample analyses. Here, we investigate four 4 years of data resulting from repeated processing of the CRONUS-N reference material for 5 cosmogenic <sup>10</sup>Be and <sup>26</sup>Al analyses. At University of Vermont, we prepared a CRONUS-N 6 sample with most of our sample batches from 2013 to 2017; these reference material samples 7 were then distributed to four different accelerator mass spectrometry facilities, yielding 73 <sup>10</sup>Be analyses and 58  $^{26}$ Al analyses. We determine CRONUS-N  $^{10}$ Be concentrations of (2.26  $\pm$  0.14) x 8  $10^5$  atoms  $g^{-1}$  (n = 73, mean, 1 SD) and  $^{26}$ Al concentrations of (1.00  $\pm$  0.08) x  $10^6$  atoms  $g^{-1}$  (n = 9 10 58, mean, 1 SD). We find a reproducibility of 6.3% for <sup>10</sup>Be and 7.7% for <sup>26</sup>Al (relative standard deviations). We also document highly variable <sup>27</sup>Al and Mg concentrations and a <sup>10</sup>Be dispersion 11 12 twice as large as the mean AMS analytic uncertainty. Analyses of the CRONUS-N material with 13 and without density separation demonstrate that non-quartz minerals are present in the material and have a large impact on measured concentrations of <sup>27</sup>Al, <sup>10</sup>Be, and impurities; these non-14 15 quartz minerals represent only a very small portion of the total mass (0.6-0.8%) but have a 16 disproportionally large effect on the resulting data. Our results highlight the importance of 17 completely removing all non-quartz mineral phases from samples prior to Be/Al extraction for 18 the determination of *in situ* cosmogenic <sup>10</sup>Be and <sup>26</sup>Al concentrations. 19

Keywords: geochronology; cosmogenic nuclides; accelerator mass spectrometry; quality control; beryllium-10

#### 1. Introduction

21

22

23

24

25

26

27

28

29

30

31

32

33

34

35

36

37

38

39

40

41

42

43

Cosmogenic nuclides have been widely used to study a variety of Quaternary surface processes (Bierman and Nichols, 2004; Gosse and Phillips, 2001; Granger et al., 2013; Nishiizumi et al., 1993; Portenga and Bierman, 2011; Schaefer et al., 2022; von Blanckenburg and Willenbring, 2014). Cosmogenic nuclide methods commonly require considerable chemical processing of the original sample material to isolate the element of interest, followed by isotopic ratio measurements by accelerator mass spectrometry (AMS). Despite the widespread use of these isotopes in Earth science (Schaefer et al., 2022), there have been relatively few studies that have used systematic intercomparison between sample preparation laboratories and AMS facilities (Fink and Smith, 2007; Merchel et al., 2012; Schnabel et al., 2007) to assess and quantify the cumulative effect of uncertainties and biases. Several new reference materials, including the materials collected and purified as part of the CRONUS-Earth project (Jull et al. (2015); standards CRONUS-A and CRONUS-N) as well as CoQtz-N (Binnie et al., 2019) and UVM-A (Corbett et al., 2019), present such an opportunity. The goal of this study, which focuses on repeated analyses of a single reference material (CRONUS-N; Jull et al. (2015)), is to explore sources of error and imprecision in sample preparation and measurement. Measurement of *in situ* produced cosmogenic nuclides, such as <sup>10</sup>Be and <sup>26</sup>Al, can provide insight about a wide range of Earth processes including the behavior of glaciers (Balco, 2011; Fabel and Harbor, 1999), the timing of recent seismic activity (Bierman et al., 1995; Brown et al., 1998; Matmon et al., 2005; Rood et al., 2010), and the erosion rates of both bedrock (Nishiizumi et al., 1991; Nishiizumi et al., 1986) and drainage basins (Bierman and Steig, 1996; Brown et al., 1995; Granger et al., 1996; von Blanckenburg, 2005). Using multiple nuclides with different half-lives provides constraints about histories involving both burial and

exposure, such as in the case of surfaces covered by non-erosive glacial ice (Bierman et al., 1999) or sediment (Granger and Muzikar, 2001). In addition to constraining burial, using multiple nuclides in tandem can illuminate exposure/erosion histories (Hidy et al., 2018) and paleoaltimetry (Blard et al., 2019). A <sup>26</sup>Al/<sup>10</sup>Be burial isochron approach (Balco and Rovey, 2008) has provided insight about long-term ice sheet history (Balco and Rovey, 2010), fluvial processes (Bender et al., 2020), and the evolution of humans (Gibbon et al., 2014; Granger, 2014). Results of cosmogenic nuclide studies are becoming increasing relevant to societal issues such as climate change, erosion, and geohazards; accuracy and reproducibility of isotope concentration measurements has thus become more important.

In association with the CRONUS-Earth project (Phillips et al., 2016), a set of reference

In association with the CRONUS-Earth project (Phillips et al., 2016), a set of reference standards was collected, purified, and distributed. Our work here focuses on CRONUS-N, a beach sand from Noosa Beach in Queensland, Australia (Jull et al., 2015). Although the CRONUS-N material is dominantly white quartz, infrequent non-quartz grains are present. According to Jull et al. (2015), the CRONUS-N material contains 236  $\mu$ g g<sup>-1</sup> total Al; the mean  $^{10}$ Be concentration of CRONUS-N, analyzed 23 times and prepared in 11 different extraction laboratories, was 2.17  $\pm$  0.09 x 10<sup>5</sup> atoms g<sup>-1</sup> (mean, 1 SD, their Table 4a, with an outlier from a 12<sup>th</sup> laboratory omitted) and the mean  $^{26}$ Al concentration, analyzed ten times and prepared in five different extraction laboratories, was 1.05  $\pm$  0.11 x 10<sup>6</sup> atoms g<sup>-1</sup> (mean, 1 SD, their Table 4b). Eight different AMS facilities were used to make these measurements.

Here, we use repeated analyses of the CRONUS-N reference material to assess the accuracy and precision of cosmogenic <sup>10</sup>Be and <sup>26</sup>Al quantification. Whereas Jull et al. (2015) focused on samples prepared at numerous different laboratories and analyzed at different AMS facilities, this study uses only samples prepared at the University of Vermont laboratory in order

to avoid methodological differences and to isolate batch-to-batch and AMS-to-AMS variability. We report and analyze the reproducibility of 73  $^{10}$ Be (Fig. 1) and 58  $^{26}$ Al (Fig. 2) measurements, each prepared individually from CRONUS-N material and made over the course of four years at four different AMS facilities. We also present data from CRONUS-N after performing density separation to remove non-quartz mineral phases, as well as data from acid-leached CRONUS-N to assess whether any leachable meteoric  $^{10}$ Be remained after initial acid treatment when the standard was prepared. Our goal is to examine the accuracy and precision of CRONUS-N measurements by exploring factors relevant during sample preparation and AMS measurement. Ultimately, we aim to improve sample preparation and measurement methodology.

#### 2. Background: Sources of Error in Cosmogenic Nuclide Data

In this paper, we focus on the uncertainty of measured cosmogenic nuclide concentrations, which encompasses both accuracy (systematic errors) and precision (random errors). Accuracy and precision are each a function of two separate processes: sample preparation during which Be and Al are isolated, and sample analysis during which <sup>10</sup>Be/<sup>9</sup>Be and <sup>26</sup>Al/<sup>27</sup>Al are measured by AMS. Both accuracy and precision encompass known factors (which are reported in analytic uncertainties) and unknown factors (which are not well-constrained); together, they comprise total uncertainty.

#### 2.1. Uncertainty from Sample Preparation Laboratories

Sample processing laboratories, where quartz is purified and then elements of interest are chemically isolated from quartz (including at University of Vermont; Corbett et al. (2016)), introduce inaccuracy in multiple ways. While some sources of inaccuracy are more

straightforward to quantify, for example by monitoring balance performance, others as explored below are harder to assess. Because sample processing encompasses two distinct phases, quartz preparation and Be/Al isolation, there are two distinct sources of error before AMS analysis begins.

Imperfect quartz purification can result in erroneous isotopic concentration measurements in several ways. Meteoric <sup>10</sup>Be, which is produced in the atmosphere and adhered to the surface of mineral grains (Willenbring and von Blanckenburg, 2010), can bias <sup>10</sup>Be concentrations if it is not completely removed from quartz grains during sample preparation (Brown et al., 1991; Kohl and Nishiizumi, 1992). Minerals other than quartz can also persist through the purification process; such minerals could have different nuclide production rates than quartz and/or could harbor meteoric <sup>10</sup>Be (Ivy-Ochs et al., 1998). Surface weathering products, including Al- and Febearing oxy-hydroxides, efficiently trap meteoric <sup>10</sup>Be and, if not fully removed, result in overestimating the true *in situ* <sup>10</sup>Be concentration (Barg et al., 1997; Graly et al., 2010). Different sample cleaning procedures (e.g., etching with higher concentrations of hydrofluoric acid as discussed in Brown et al. (1991)) may have different efficacy at removing meteoric <sup>10</sup>Be adhered to non-quartz minerals; certain quartz digestion procedures (e.g., room-temperature digestion as discussed in Merchel et al. (2019)) may be more useful for leaving behind non-quartz mineral phases as residue.

During Be/Al extraction, some sources of inaccuracy, such as weighing errors, are likely small and random; other sources, such as quantification of the concentration of the <sup>9</sup>Be carrier solution added to every sample, are likely larger and have the potential to bias results systematically. For <sup>26</sup>Al analysis, additional uncertainty is introduced because the total amount of <sup>27</sup>Al in the digested sample (the sum of native <sup>27</sup>Al in processed quartz and <sup>27</sup>Al added through

carrier as needed) is most often quantified by Inductively-Coupled Plasma Optical Emission Spectrometry (ICP-OES), with uncertainties of one to several percent (Corbett et al., 2016). ICP-OES analyses may be biased if the <sup>27</sup>Al is not fully taken up in solution as a mono-atomic ion but instead partially remains as a complex fluoride, or if the ICP-OES standards are not matrix-matched to the sample material (Bierman and Caffee, 2002; Fujioka et al., 2015; Ruszkiczay-Rüdiger et al., 2021).

In addition to affecting accuracy, sample processing procedures can also affect precision. Laboratory backgrounds (contamination), as quantified by processed blanks, can decrease precision because the absolute uncertainties in sample and blank measurement are propagated in quadrature. This is especially the case for samples with low concentrations of cosmogenic nuclides because the blank correction and propagated uncertainty are large in relation to the sample ratio. The consistency of process blanks in a sample preparation laboratory also plays a role, with larger blank variability leading to higher blank uncertainty and therefore decreased precision. Contamination with other elements (e.g., Al or Ti in a Be sample) can reduce AMS counting efficiency, which impacts precision (Hunt et al., 2008; Merchel et al., 2008).

## 2.2. Uncertainty from AMS Laboratories

After sample preparation, isotopic analysis occurs by AMS (Muzikar et al., 2003; Tuniz et al., 1998), which adds an additional source of uncertainty. All samples are measured in relation to primary standards such as the 07KNSTD dilution series (Nishiizumi et al., 2007). The accuracy of sample measurement is controlled by matrix effects (Hunt et al., 2006; Merchel et al., 2008), cathode geometry (Hunt et al., 2007; Rood et al., 2013; Shanks and Freeman, 2015), and both instrument and target performance during measurement (Hunt et al., 2008). The

precision of AMS analysis is controlled by Poisson counting statistics, with greater numbers of counts of the rare isotope yielding more precise analyses (Rood et al., 2013; Rood et al., 2010). Precision is also dictated by reproducibility between repeated AMS measurements, particularly for samples with higher ratios for which the counting statistics are less important (Rood et al., 2014). Correction for the influence of isobars, such as <sup>10</sup>B and <sup>26</sup>Mg, can impact both the precision and the accuracy of <sup>10</sup>Be and <sup>26</sup>Al measurements (Merchel et al., 2012).

From 2013 to 2017, we prepared one aliquot ( $10.8 \pm 1.5$  g, mean, n = 73, 1 SD;

## 3. Study Design

Supplemental Data Table S1) of CRONUS-N material as part of most of our sample preparation batches (which consisted of ten unknowns, one processed blank, and one CRONUS-N aliquot).

We did not conduct any further preparation of the CRONUS-N material, but used it as supplied by Jull et al. (2015). Over the duration of the experiment, we processed 73 batches of samples that included CRONUS-N, with AMS analyses spanning October 2013 through August 2017.

Resulting <sup>10</sup>Be (Fig. 1; Supplemental Data Table S2) and <sup>26</sup>Al (Fig. 2; Supplemental Data Table S3) analyses took place at four different AMS facilities: Australian Nuclear Science and Technology Organization (ANSTO), Lawrence Livermore National Laboratory (LLNL), Purdue Rare Isotope Measurement (PRIME) Laboratory, and Scottish Universities Environmental Research Centre (SUERC).

Based on the results of the above analyses, we conducted three additional follow-up experiments targeted at assessing whether the small portion of non-quartz mineral phases in CRONUS-N (~0.6-0.8% by mass, as determined through density separation) impacted <sup>10</sup>Be and <sup>26</sup>Al concentrations. First, to assess cosmogenic nuclide concentrations of the different mineral

phases, we conducted density separation on three aliquots of CRONUS-N material and analyzed the isotopic concentrations of the dissolved quartz and the dense mineral phases separately; we refer to this as the "dissolution experiment" below. Second, to assess whether meteoric <sup>10</sup>Be is disproportionately adhered onto the surfaces of the dense minerals, we conducted additional CRONUS-N density separation, leached separately both the quartz and dense separates in 6N HCl acid to remove any remaining grain coatings, and analyzed the isotopic concentrations of the leachates; we refer to this as the "leaching experiment" below. Finally, we conducted Scanning Electron Microscope (SEM) analysis of density-separated CRONUS-N material to examine the composition and condition of the non-quartz mineral phases.

For all CRONUS-N samples, we gathered various quality control and performance metrics (Supplemental Data Table S2). Once the Be and Al fractions had been separated and prior to their precipitation into hydroxide gels, we removed small aliquots of the solutions for quantifying yield and purity using ICP-OES. During AMS analysis, we recorded the <sup>9</sup>Be beam current resulting from the sample. To remove run-to-run and lab-to-lab variability in AMS performance, we normalized the sample beam current to the mean of primary standard beam currents analyzed at the same time using the beam current normalization approach outlined in Corbett et al. (2016).

One blank was processed in each batch of samples and analyzed at the same AMS and at the same time as the associated CRONUS-N sample (Supplemental Data Tables S5 and S6). Due to the long duration of the study period, the  $^{10}$ Be/ $^{9}$ Be blanks (Supplemental Data Table S5) encompassed eight different beryl carriers; all carriers were made at University of Vermont from the same crushed beryl crystal using the same method. We explore and compare two options for the  $^{10}$ Be/ $^{9}$ Be blank correction below: (1) an AMS-by-AMS blank that uses the mean of all blanks

prepared and analyzed alongside CRONUS-N samples at each facility, and (2) a batch-by-batch blank that uses the single blank in each batch. For <sup>26</sup>Al/<sup>27</sup>Al blanks (Supplemental Data Table S6), all samples were spiked with the same SPEX stable isotope carrier, so we use an AMS-by-AMS blank to correct all <sup>26</sup>Al/<sup>27</sup>Al analyses.

186

187

188

189

190

191

192

193

194

195

196

197

198

199

200

201

202

203

204

182

183

184

185

# 4. Sample Preparation and Analysis Methods

#### 4.1. Be and Al Isolation

All samples were prepared at University of Vermont following standard procedures (Corbett et al., 2016). We used the original CRONUS-N material as supplied by the CRONUS-Earth project, which was magnetically-separated and acid-etched before distribution (Jull et al., 2015). We added ~250 μg <sup>9</sup>Be (Supplemental Data Table S1) to each CRONUS-N sample using beryl carrier made at University of Vermont but did not add <sup>27</sup>Al carrier due to the relatively high native <sup>27</sup>Al concentrations in the CRONUS-N material (~300 µg g<sup>-1</sup>, as detailed in Section 6.4). For blanks, we added  $\sim 250 \mu g^9$ Be and  $\sim 1500 \mu g^{27}$ Al. We digested the CRONUS-N material in ~100mL concentrated hydrofluoric acid, steadily increasing the temperature over a period of several days to 135°C, then let the samples stay at the terminal temperature for two to three days. We quantified total <sup>27</sup>Al in the samples immediately following digestion with ICP-OES analysis of replicate aliquots (representing  $\sim 2\%$  and  $\sim 4\%$  of the sample, respectively) using two emission lines (308.215 and 309.271 nm) and an internal standard (Ga or Y; Supplemental Data Table S1). This ICP-OES analysis also served to verify that no native <sup>9</sup>Be (i.e., <sup>9</sup>Be originally in the CRONUS-N material, not added through carrier) was present in the material. In all cases for Be and some cases for Al, the CRONUS-N samples were analyzed by

AMS along with the samples and blank in their associated batch. In cases where Al analysis was

not part of the original project, we analyzed the CRONUS-N and the associated Al blank independent of the samples for the purposes of this study.

Samples for which the Al fraction would be analyzed at ANSTO, LLNL, and SUERC followed our standard cation column chromatography procedure (Corbett et al., 2016). Samples for which the Al fraction would be analyzed at PRIME underwent Mg removal as described in Corbett et al. (2017) because the <sup>26</sup>Mg isobar interferes with <sup>26</sup>Al measurement on the PRIME gas-filled magnet if the <sup>26</sup>Mg count rate is high (Caffee et al., 2015; Granger et al., 2014). In certain cases, archived Al fractions were reconstituted and then underwent a second cation column chromatography procedure for Mg removal before analysis at PRIME (Corbett et al., 2017).

## 4.2. Follow-Up Experiments

For the two follow-up experiments targeted at understanding cosmogenic nuclide concentrations in the non-quartz mineral phases, we conducted heavy liquid density separation of the CRONUS-N material using LST heavy liquid with a density of 2.85 g mL $^{-1}$ . In both cases, we used  $\sim 33$  g of CRONUS-N material, which yielded  $\sim 0.2$  g of non-quartz minerals. For each of the two experiments, we split the  $\sim 33$  g of separated quartz into three aliquots in order to mimic the  $\sim 10$ -11 g CRONUS-N samples processed throughout the duration of the study. Given the small mass of the dense fraction, for each follow-up experiments we used the full  $\sim 0.2$  g of dense mineral phases as a single sample to maximize the likelihood that there would be sufficient cosmogenic nuclides to be detectable by AMS.

For the dissolution experiment (<sup>10</sup>Be and <sup>26</sup>Al), we processed the three aliquots of density-separated quartz, as well as one aliquot of amalgamated dense mineral phases, using

standard *in situ* sample processing techniques as described above. Because the four resulting samples were analyzed at PRIME for both isotopes, we performed blank corrections based on the overall mean PRIME <sup>10</sup>Be/<sup>9</sup>Be and <sup>26</sup>Al/<sup>27</sup>Al blanks.

For the leaching experiment (<sup>10</sup>Be only), we leached the three quartz separates and the aliquot of amalgamated dense mineral phases in 30 mL of 6N hydrochloric acid for 48 hours at 98 °C after adding our usual <sup>9</sup>Be carrier spike. After cooling the samples, we decanted the liquid and cleaned it of Fe, Ti, and Al using our standard *in situ* sample column procedures. Because the four resulting samples were analyzed at LLNL, we performed blank corrections based on the overall mean LLNL <sup>10</sup>Be/<sup>9</sup>Be blank.

To explore the mineralogy of the non-quartz grains in CRONUS-N in more detail, we conducted SEM analysis of a polished grain mount of minerals isolated through density separation. We made observations on the relative abundance of non-quartz mineral grains and used Energy Dispersive Spectroscopy (EDS) to analyze mineral compositions and ultimately make mineral identifications. We also collected high-resolution images of grain fractures and other alteration features.

## 4.3. Accelerator Mass Spectrometry Analysis

Ratios of <sup>10</sup>Be/<sup>9</sup>Be and <sup>26</sup>Al/<sup>27</sup>Al were analyzed at ANSTO (n = 9 and 11, respectively), LLNL (n = 20 and 14), PRIME (n = 11 and 20), and SUERC (n = 33 and 13), yielding a total of 73 <sup>10</sup>Be/<sup>9</sup>Be measurements (Supplemental Data Table S2) and 58 <sup>26</sup>Al/<sup>27</sup>Al measurements (Supplemental Data Table S3). ANSTO and SUERC use back-packing cathodes, whereas LLNL and PRIME use front-packing cathodes. <sup>10</sup>Be/<sup>9</sup>Be analyses were normalized to primary standard 07KN-5-2 at ANSTO (reference value 8.56 x 10<sup>-12</sup>), 07KNSTD3110 at LLNL and PRIME

(Nishiizumi et al. (2007);  $2.85 \times 10^{-12}$ , also known as 07KN-5-4), and NIST-4325 at SUERC (2.79 x  $10^{-11}$ ).  $^{26}Al/^{27}Al$  analyses were normalized to primary standard KN-4-2 at ANSTO (reference value  $3.096 \times 10^{-11}$ ), KNSTD30960 at LLNL and PRIME (Nishiizumi (2004);  $1.82 \times 10^{-12}$ , also known as KN-5-2), and Z92-0222 at SUERC (assumed  $4.11 \times 10^{-11}$ ). These standards are self-consistent to <1% for Be and <2% for Al (Fink and Smith, 2007).

At SUERC, CRONUS-N samples were analyzed differently than at the other three facilities because a correlation between measured <sup>10</sup>Be/<sup>9</sup>Be ratio and beam current has been observed at the SUERC AMS (Balco et al., 2021). We sputtered the CRONUS-N samples and primary standards used for normalization for the same durations of time during every run of each individual cathode in order to minimize any systematic errors or biases in isotope ratio measurements due to variations in sample sputtering-related factors. For the SUERC data presented here, we present both the original data as well as data normalized to remove current dependence as described in Balco et al. (2021).

#### 5. Blank Ratios, Blank Correction, and Sensitivity Analysis

For both isotopes, AMS-measured blank ratios (Supplemental Data Tables S5 and S6) are two orders of magnitude smaller than sample ratios, indicating that the blank correction represents a small portion (~1%) of the sample ratio. For  $^{10}$ Be/ $^{9}$ Be, the mean blank ratio is (2.6  $\pm$  2.7) x  $10^{-15}$  (n = 71 analyses at four AMS facilities), while the mean uncorrected CRONUS-N sample ratio is (1.54  $\pm$  0.29) x  $10^{-13}$  (n = 73). For  $^{26}$ Al/ $^{27}$ Al, the mean blank ratio is (2.3  $\pm$  4.0) x  $10^{-15}$  (n = 57 analyses at four AMS facilities), while the mean uncorrected CRONUS-N sample ratio is (1.54  $\pm$  0.28) x  $10^{-13}$  (n = 58). For both isotopes, we subtract blank ratios from sample ratios and propagate the uncertainties in quadrature.

The eight different beryl carriers, when analyzed as process blanks over the study period, have overlapping populations of <sup>10</sup>Be/<sup>9</sup>Be ratios (Fig. 3). Each population has a large spread (mean relative standard deviation (RSD) of 45%), due primarily to poor counting statistics associated with the low <sup>10</sup>Be/<sup>9</sup>Be ratios; many of these analyses had only several <sup>10</sup>Be counts, resulting in large uncertainties and thus poor replication.

When different possible blank corrections are applied to the  $^{10}$ Be/ $^{9}$ Be data, there is little difference in the resulting calculated sample  $^{10}$ Be concentration. Comparing an AMS-by-AMS blank correction versus a batch-by-batch blank correction yields a mean difference of 0.1% at ANSTO (n = 9), 0.3% at LLNL (n = 20), 0.2% at PRIME (n = 11), and 1.6% at SUERC (n = 30). These are considerably smaller sources of uncertainty than the AMS counting statistics for  $^{10}$ Be and the overall  $^{10}$ Be dispersion, as explored in the following section. We choose to use the AMS-by-AMS blank correction, but note that applying a batch-by-batch blank correction instead would have minimal impact on the calculated  $^{10}$ Be concentrations and resulting conclusions.

#### 6. Results

#### 6.1. SEM Analysis

SEM observations (Supplemental Data Figs. S1-S5) and EDS analysis (Supplemental Data Fig. S6) confirm that the CRONUS-N material contains non-quartz mineral phases. The most abundant non-quartz mineral phases we observed are tourmaline and rutile; we also observed garnet, spinel (with varying compositions, including chromite), zircon, ilmenite, and a rare Earth element-bearing aluminum phosphate that we hypothesize is florencite (Supplemental Data Figs. S1-S3 and S6). We found that some of the tourmaline grains are heavily altered and exhibit dense, cross-cutting fractures (Supplemental Data Fig. S4). Some rutile grains exhibit

indications of varying degrees of alteration and porous textures (Supplemental Data Fig. S5), and we noted grains of intergrown rutile and quartz (Supplemental Data Fig. S1).

#### 6.2. SUERC Beam Current Correction

For CRONUS-N  $^{10}$ Be/ $^{9}$ Be measured at SUERC,  $^{10}$ Be concentrations are (2.21 ± 0.15) x  $^{105}$  atoms  $^{-1}$  (n = 33). When the beam current correction described in Balco et al. (2021) is applied, corrected  $^{10}$ Be concentrations are (2.23 ± 0.12) x  $^{105}$  atoms  $^{-1}$ . The two populations are indistinguishable using a two-tailed, unequal variance t-test (p = 0.67), but the RSD decreases from 6.7% to 5.3%. Because the correction factor of Balco et al. (2021) is based on a single study and does not significantly alter our interpretations, we choose to use the uncorrected  $^{10}$ Be concentrations for the analyses below.

# 6.3. CRONUS-N <sup>10</sup>Be

Measured  $^{10}$ Be concentrations of CRONUS-N reference material (Table 1 and Supplemental Data Table S2) range from (1.93 to 2.55) x  $10^5$  atoms  $g^{-1}$  (Fig. 1), with a mean of (2.26  $\pm$  0.14) x  $10^5$  atoms  $g^{-1}$  (n = 73, 1 SD). This is higher and statistically separable (p < 0.01, two-tailed unequal variance t-test) from the results of Jull et al. (2015), who reported a mean value of (2.17  $\pm$  0.09) x  $10^5$  atoms  $g^{-1}$  (n = 23, 1 SD). The spread of our data is greater (RSD 6.3%) than that of Jull et al. (2015) (RSD 4.1%).

Across the four different AMS laboratories (Fig. 1 and Table 1), the measured  $^{10}$ Be concentrations form separable populations based on a one-way ANOVA (p = 0.02). Tukey's Test shows that  $^{10}$ Be concentrations based on data from SUERC are distinguishable from those from ANSTO and PRIME (p = 0.05 for both), but that no other pairings are separable. If we instead

use the beam current corrected SUERC data, the overall ANOVA and Tukey's Test results are the same. The spread in RSD of <sup>10</sup>Be concentrations grouped by AMS is small and ranges from 5.0 to 6.7% (or 5.0 to 5.7% if we use the beam current corrected SUERC data).

The mean AMS analytic measurement uncertainty as reported by each AMS facility for all of the  $^{10}$ Be/ $^{9}$ Be measurements is  $(3.1 \pm 0.9)$  % (n = 73, 1 SD, Table 1). This varies between different AMS laboratories and is statistically separable (one-way ANOVA, p <0.01); analytic uncertainty grouped by AMS ranges from 2.1 to 3.6% (Table 1). Tukey's Test shows that the analytic uncertainty is separable between all pairings (p < 0.05), except ANSTO with PRIME and PRIME with SUERC. The  $^{10}$ Be/ $^{9}$ Be AMS analytic measurement uncertainty is appreciably smaller than the RSD of the  $^{10}$ Be concentrations calculated from these ratios; the dispersion, defined as the ratio of the RSD of the calculated  $^{10}$ Be concentrations to the mean AMS measurement uncertainty, is 1.7-2.4 for the different AMS laboratories, or 2.0 for the dataset as a whole (Table 1, Fig. 4). This relatively large dispersion implies sources of variance beyond AMS measurement uncertainty.

# 6.4. CRONUS-N $^{27}Al$ and $^{26}Al$

Measured CRONUS-N  $^{27}$ Al concentrations (Fig. 5 and Supplemental Data Table S1), as quantified by ICP-OES immediately following digestion, are 219 to 417  $\mu$ g g<sup>-1</sup>, averaging 309  $\pm$  46  $\mu$ g g<sup>-1</sup> (n = 58, 1 SD). This represents an RSD of 14.9%. Using the current methods at University of Vermont, our mean analytic error during ICP-OES analyses is ~2% (Corbett et al., 2016), implying a dispersion of 7.5.

Measured  $^{26}$ Al concentrations of CRONUS-N material (Table 1 and Supplemental Data Table S3) are (0.85 to 1.16) x  $10^6$  atoms  $g^{\text{-}1}$  (Fig. 2), averaging (1.00  $\pm$  0.08) x  $10^6$  atoms  $g^{\text{-}1}$  (n =

58, 1 SD). This is statistically indistinguishable (p = 0.19, two-tailed unequal variance t-test)
from the results of Jull et al. (2015), who reported a mean value of (1.05 ± 0.11) x 10<sup>6</sup> atoms g<sup>-1</sup>
(n = 10, 1 SD). Unlike for <sup>10</sup>Be, our data have a smaller spread of <sup>26</sup>Al concentrations (RSD
7.7%) than those of Jull et al. (2015) (RSD 10.1%).

Across the four different AMS laboratories (Fig. 2 and Table 1), the measured  $^{26}$ Al concentrations form separable populations based on a one-way ANOVA (p = 0.03). Tukey's Test shows that  $^{26}$ Al concentrations based on data from LLNL are distinguishable from those from PRIME (p = 0.05) and SUERC (p = 0.04), and that no other pairings are separable. The spread in RSD of  $^{26}$ Al concentrations grouped by AMS is larger than that observed for  $^{10}$ Be and is greater for LLNL and PRIME (8.1 and 8.4%, respectively) than for ANSTO and SUERC (5.7 and 5.1%).

The mean analytic AMS measurement uncertainty as reported by each AMS facility for all of the  $^{26}$ Al/ $^{27}$ Al measurements is  $(6.7 \pm 3.1)$  % (n = 58, 1 SD, Table 1). This varies between different AMS laboratories and is statistically separable (one-way ANOVA, p <0.01); analytic uncertainty grouped by AMS ranges from 4.2 to 10.5% (Table 1). Tukey's Test shows that the analytic uncertainty is separable between all pairings (p < 0.05), except ANSTO with PRIME and ANSTO with SUERC. Unlike for  $^{10}$ Be/ $^{9}$ Be, the  $^{26}$ Al/ $^{27}$ Al analytic uncertainties are similar to the RSD of calculated  $^{26}$ Al concentrations; the dispersion is 0.8-1.3 for the different AMS laboratories, or 1.1 for the dataset as a whole (Table 1, Fig. 4).

# 6.5. CRONUS-N <sup>26</sup>Al/<sup>10</sup>Be

Calculated  $^{26}$ Al/ $^{10}$ Be ratios are 3.56 to 5.31, averaging 4.48  $\pm$  0.42 (n = 58, 1 SD, Supplemental Data Table S4). This is statistically separable (p < 0.01, two-tailed unequal

variance t-test) from the results of Jull et al. (2015), whose data suggest  $4.93 \pm 0.35$  (n = 9, 1 SD, based on our calculations because  $^{26}$ Al/ $^{10}$ Be ratios are not directly reported). Our data have a larger spread of calculated  $^{26}$ Al/ $^{10}$ Be ratios (RSD 9.3%) than those of Jull et al. (2015) (RSD 7.0%). We do not present comparisons between AMS laboratories here because the  $^{10}$ Be and  $^{26}$ Al analyses of the same aliquot of material were frequently conducted at different facilities.

The mean uncertainty (including propagation of the uncertainty for each isotope) for all of the  $^{26}$ Al/ $^{10}$ Be ratios is  $(7.5 \pm 3.0)$  % (n = 58, 1 SD), dominated by the proportionally larger  $^{26}$ Al uncertainty. The  $^{26}$ Al/ $^{10}$ Be measurement uncertainty is slightly smaller than the RSD of the calculated  $^{26}$ Al/ $^{10}$ Be ratios, with an overall dispersion of 1.2.

6.6. CRONUS-N <sup>10</sup>Be and <sup>26</sup>Al After Density Separation (Dissolution Experiment Part 1)

The  $^{27}$ Al concentration of CRONUS-N quartz following density separation is  $149 \pm 2 \mu g$   $g^{-1}$  (mean, n = 3, 1 SD; Fig. 5), yielding an RSD of 1.3%. This is about half the concentration of  $^{27}$ Al that existed in the material before density separation (mean  $309 \pm 46 \mu g g^{-1}$ , RSD 15%), and the variability in  $^{27}$ Al concentration is an order of magnitude smaller.

For the three aliquots of CRONUS-N material on which we performed density separation and processed the samples using standard *in situ* methods,  $^{10}$ Be concentrations in this purified quartz measured at PRIME are  $(2.03 \pm 0.07)$ ,  $(2.21 \pm 0.07)$ , and  $(2.10 \pm 0.07)$  x  $10^5$  atoms g<sup>-1</sup> (Fig. 6), yielding a mean of  $(2.11 \pm 0.09)$  x  $10^5$  atoms g<sup>-1</sup>. When compared to other  $^{10}$ Be analyses at PRIME only, the  $^{10}$ Be concentrations of CRONUS-N material with  $((2.11 \pm 0.09) \times 10^5$  atoms g<sup>-1</sup>, n = 3) and without  $((2.34 \pm 0.13) \times 10^5$  atoms g<sup>-1</sup>, n = 11) density separation are statistically separable (p = 0.02, two-tailed unequal variance t-test). The RSD of the measurements of density separated material is 4.1%, which is similar to the mean analytic uncertainty (3.3%). Unlike the

 $^{10}$ Be concentrations of the unseparated CRONUS-N material, the  $^{10}$ Be concentrations of this density separated material are similar to the measurements reported in Jull et al. (2015); the two populations are statistically indistinguishable (p = 0.39, two-tailed unequal variance t-test).

 $^{26}$ Al concentrations of CRONUS-N material after density separation are  $(1.18 \pm 0.05)$ ,  $(1.11 \pm 0.05)$ , and  $(1.11 \pm 0.05)$  x  $10^6$  atoms  $g^{-1}$ , yielding a mean of  $(1.13 \pm 0.04)$  x  $10^6$  atoms  $g^{-1}$ . Unlike for  $^{10}$ Be, the  $^{26}$ Al concentration after density separation  $((1.13 \pm 0.04) \times 10^6 \text{ atoms } g^{-1}, n = 3)$  is greater than in the sample material without density separation  $((1.02 \pm 0.09) \times 10^6 \text{ atoms } g^{-1}, n = 20)$ . These data form statistically separable populations (p < 0.01, two-tailed unequal variance t-test, PRIME data only). The RSD of the measurements of separated material is 3.2%, which smaller than the mean analytic uncertainty (4.6%).

# 6.7. CRONUS-N Dense Fraction (Dissolution Experiment Part 2)

Heavy liquid density separation of 34.092 g CRONUS-N material yielded 0.197 g of non-quartz minerals, or about 0.6% by mass. The non-quartz mineral phases resulting from the three density separations described above were combined to yield sufficient material for one analysis. The  $^{10}$ Be concentration of the amalgamated non-quartz fraction is  $(4.55 \pm 0.23) \times 10^6$  atoms g<sup>-1</sup>, or about 22 times higher than the associated quartz. Visual observation suggested that all of the dense material dissolved in concentrated HF at 135 °C. A simple mixing model, which incorporates the mass and  $^{10}$ Be concentrations of the separated quartz and dense fractions when measured separately, predicts that a CRONUS-N sample with 0.6% dense material by mass should have a  $^{10}$ Be concentration of 2.36 x  $^{10}$ 5 atoms g<sup>-1</sup>; this prediction replicates almost exactly what we measured for the unseparated CRONUS-N material  $((2.34 \pm 0.13) \times 10^5) \times 10^5$  atoms g<sup>-1</sup>, n = 11, PRIME only). We calculate that in the CRONUS-N material, as supplied and with no

additional purification, the <sup>10</sup>Be residing within the non-quartz mineral phases (including any residual meteoric <sup>10</sup>Be that may persist; see Section 6.7) accounts for 11% of the total measured <sup>10</sup>Be atoms.

In contrast, the  $^{26}$ Al concentration of the non-quartz minerals is low and the mass was small, allowing us to obtain only an upper limit. ICP-OES analysis indicated that the separated, dense material contained 7109 µg of total Al (with no carrier added), or about 3.6% by mass of the 0.197 g sample. The measured  $^{26}$ Al/ $^{27}$ Al ratio is  $(2.6 \pm 3.8) \times 10^{-16}$ . To obtain an upper bound, we apply a  $2\sigma$  uncertainty to the measured  $^{26}$ Al/ $^{27}$ Al with the assumption that all  $^{26}$ Al counts came from the sample itself. This yields an upper limiting  $^{26}$ Al/ $^{27}$ Al of 1.0 x  $^{26}$ Al concentration of <8 x  $^{26}$ Al atoms  $^{26}$ 

# 6.8. CRONUS-N Meteoric <sup>10</sup>Be (Leaching Experiment)

Heavy liquid density separation of 32.430 g CRONUS-N material yielded 0.252 g non-quartz minerals, or about 0.8% by mass. For the three aliquots of density-separated quartz, meteoric  $^{10}$ Be concentrations of the resulting leachate measured at LLNL yield  $^{10}$ Be/ $^9$ Be ratios of  $^{\sim}10^{-15}$ , indistinguishable from background levels. For the one aliquot of amalgamated dense material, the  $^{10}$ Be/ $^9$ Be ratio is  $(2.8 \pm 0.2) \times 10^{-15}$ , which converts to a  $^{10}$ Be concentration of  $(1.14 \pm 0.45) \times 10^5$  atoms g<sup>-1</sup>.

Given that the non-quartz minerals represented  $\sim 0.8\%$  of the total CRONUS-N mass in this experiment and our typical CRONUS-N sample was 10.8 g (mean, n = 73), we infer that the average CRONUS-N sample contained  $\sim 0.09$  g non-quartz minerals. We conclude that in CRONUS-N, the acid-leachable  $^{10}$ Be adsorbed onto the surface of non-quartz mineral phases accounts for  $\sim 0.5\%$  of the total measured  $^{10}$ Be atoms. This mass portion of non-quartz minerals,

coupled with their  $^{10}$ Be concentration, is sufficient to add  $\sim 1000$  atoms  $g^{-1}$  of leachable meteoric  $^{10}$ Be to each  $\sim 11$  g CRONUS-N aliquot.

# 6.9. Quality Control Metrics

The CRONUS-N samples prepared for this study had generally high and uniform Be yields. The yields of the final Be fractions were  $210 \pm 17~\mu g$  Be (n = 71 CRONUS-N analyses, with two samples excluded due to ICP failure). Samples were spiked with ~240-250  $\mu g$  Be, but 6% of each sample was removed for stable isotope quantification, so this represents a ~89-93% yield of the total possible Be. There are no significant correlations between final Be yield and calculated <sup>10</sup>Be concentration at any of the four AMS facilities, nor are there any significant correlations between final Be yield and <sup>9</sup>Be beam current. The lack of correlations with Be yield is likely due in large part to the high, consistent Be yield of the samples assessed in this study.

At three of the four AMS facilities, the final purity of the Be fraction before precipitation as the hydroxide (as evidenced by total Mg content, which we use as a proxy for impurity; Supplemental Data Table S2) has a significant relationship with the calculated  $^{10}$ Be concentration (Fig. 7). This is the case at ANSTO ( $R^2 = 0.66$ , n = 7, p = 0.03), LLNL ( $R^2 = 0.48$ , n = 20, p < 0.01), and SUERC ( $R^2 = 0.36$ , n = 32, p < 0.01). For SUERC, the relationship changes slightly if we use the beam current corrected data, but is still significant ( $R^2 = 0.24$ , R = 32, R = 0.03). There was no significant relationship between Mg content and  $R^{10}$ Be concentration at PRIME ( $R^2 = 0.26$ , R = 11, R = 0.11), although we note that this regression has a similar slope to the other three despite its poorer correlation. The spread in Mg masses for the samples after column chemistry but before final precipitation was several hundred to a thousand R = 0.250 R = 0.26 R =

because we conducted these analyses before precipitation of the hydroxide gels, this does not represent the amount of Mg that was in the AMS cathodes.

At three of the four AMS facilities, the normalized <sup>9</sup>Be beam current (used here as a proxy for sample quality; Supplemental Data Table S2) has no significant relationship with the calculated <sup>10</sup>Be concentration (Fig. 8). But at SUERC, <sup>9</sup>Be beam current (normalized to standard currents) is positively correlated with <sup>10</sup>Be concentration (R<sup>2</sup> = 0.38, n = 33, p < 0.01). Because all samples and primary standards at SUERC were sputtered for the same duration of time during each individual run of each cathode, this effect is not a product of sputtering-related factors (e.g., duration of sputtering or changes in sputtering geometry such as penetration depth into the sample material). Rather, the observed correlation between normalized beam current and <sup>10</sup>Be concentration is likely a result of non-sputtering related factors such as impurities in sample material, which caused variations in beam emittance, ion beam transport, or detector efficiency. The correlation between impurities (using Mg as a proxy; Fig. 7) and <sup>10</sup>Be concentration suggests that variable sample purity is a reasonable explanation for the systematic biases in isotope ratio measurements at SUERC.

#### 7. Discussion

#### 7.1. Heterogeneity of CRONUS-N Material

Numerous lines of evidence indicate that the CRONUS-N reference material is heterogeneous for <sup>10</sup>Be, <sup>27</sup>Al, and <sup>26</sup>Al. First, the spread of measured <sup>10</sup>Be concentrations considerably exceeds the analytic uncertainties (Fig. 4), implying additional sources of <sup>10</sup>Be variability beyond AMS counting statistics. Second, performing density separation on the CRONUS-N material reduced <sup>27</sup>Al concentrations by 50% and decreased <sup>27</sup>Al variance by a

factor of ten (Fig. 5), confirming the visual observation that non-quartz mineral phases (which must be Al-bearing in this case) are present at varying concentrations in CRONUS-N. This is supported by the high abundance of tourmaline and the presence of spinel, both of which are Albearing, that we observed by SEM (Supplemental Data Figs. S1-S3 and S6) in the non-quartz fraction. Third, analyses of CRONUS-N quartz dissolved after density separation have appreciably lower concentrations of <sup>10</sup>Be, by about 10%, in comparison to the unseparated material (Fig. 6); this is consistent with the finding that the isolated, dissolved non-quartz mineral phases have 22 times as much <sup>10</sup>Be as the quartz. Fourth, the significant positive relationship between Mg (a proxy for total impurities) and measured <sup>10</sup>Be concentration at three of the four AMS facilities (Fig. 7) reinforces the conclusion that the Mg-bearing and <sup>27</sup>Albearing non-quartz phases are driving the observed scatter in cosmogenic nuclide concentrations.

It appears that the heterogeneity of the CRONUS-N material cannot be attributed to a single non-quartz mineral phase, but rather to numerous non-quartz phases with different compositions. SEM analysis indicates that Mg-bearing tourmaline, garnet, and spinel are present (Supplemental Data Figs. S1-S3 and S6), which likely explains the high concentration and large scatter of Mg measured in the final solution before Be hydroxide precipitation (mean  $456 \pm 185$  µg, n = 73, 1 SD, Fig. 7); comparatively, the CRONUS-N aliquots on which we performed density separation had over an order of magnitude less Mg in the final Be fraction (mean  $38 \pm 19$  µg, n = 3, 1 SD). The presence of mafic minerals at least partially explains the differences in  $^{27}$ Al and Mg concentrations we measured. However, it is difficult to explain the  $^{10}$ Be concentration differences (22 times more in the dense fraction) based solely on differing *in situ* nuclide production rates, given that the  $^{10}$ Be production rates in the dense, mostly silicate minerals are

likely not appreciably different than in quartz, as inferred from elemental production rates (Leya and Michel, 2011).

# 7.2. Elevated Meteoric <sup>10</sup>Be in Non-Quartz Grains

The most likely explanation for elevated <sup>10</sup>Be in the non-quartz mineral phases is the presence of atmospherically-produced meteoric <sup>10</sup>Be, which adheres to the outsides of mineral grains (Willenbring and von Blanckenburg, 2010) and can penetrate into cracks and weathered zones in minerals (Ivy-Ochs et al., 1998). Meteoric <sup>10</sup>Be is generally removed by strong, hot hydrochloric acid treatments conducted at the beginning of quartz purification (Kohl and Nishiizumi, 1992). Our leaching experiment shows that the preparation of CRONUS-N effectively removed meteoric <sup>10</sup>Be from the quartz, but that small amounts of leachable <sup>10</sup>Be remained on or in the non-quartz mineral phases. However, such leachable <sup>10</sup>Be was minimal, as it increased the total <sup>10</sup>Be concentration by only ~0.5%; in contrast, completely dissolving the non-quartz mineral phases increased the total <sup>10</sup>Be concentration by ~10%. We hypothesize that meteoric <sup>10</sup>Be is more readily retained in heavily-altered grains like the tourmaline and rutile we observed by SEM (Supplemental Data Figs. S4 and S5), which contain abundant fractures and other alteration features that could harbor weathering products even after hydrochloric acid etching.

The lack of measurable <sup>26</sup>Al in the non-quartz mineral phases is diagnostic of the meteoric source of <sup>10</sup>Be. This is because <sup>26</sup>Al is produced only very negligibly in the atmosphere, at a rate about three orders of magnitude slower than <sup>10</sup>Be (Auer et al., 2007). Together, all of these observations strongly suggest that the <sup>10</sup>Be excess we measured in fully dissolved aliquots of non-quartz mineral phases is primarily of meteoric origin. This excess <sup>10</sup>Be resides deep in

non-quartz grains, perhaps within cracks or in secondary minerals created by weathering. Given that meteoric <sup>10</sup>Be seems to exist mostly in non-leachable forms in the dense mineral phases, removing non-quartz phases completely from all weathered samples before dissolution and isotopic analysis is a critical prerequisite for accurate determination of *in situ* <sup>10</sup>Be concentrations.

In situ production of  $^{10}$ Be in non-quartz mineral phases cannot account for the 22-fold concentration difference between quartz and non-quartz fraction, presuming that all silicate minerals have grossly similar production rates of *in situ*  $^{10}$ Be. Sediment on Noosa Beach, where CRONUS-N was collected, is supplied by rivers draining the adjacent coastal plane and low-elevation uplands. The largest catchment near Noosa is the Maroochy River, the highest point of which is about 450 m asl. Codilean et al. (2021) provide erosion rate data for the Mary and Stanley rivers near Noosa, which are eroding at  $\sim$ 8-40 m My $^{-1}$ . In the non-quartz fraction of CRONUS-N, we measured  $4.55 \pm 0.23 \times 10^6$  atoms  $g^{-1}$   $^{10}$ Be; this is about half of the saturation value for surface exposure at 450 m elevation and 26 degrees latitude and thus incompatible with even the lowest erosion rates measured in the area. Therefore, even if the non-quartz mineral phases we analyzed were sourced from the highest elevation, lowest erosion rate regions of the catchment, they would not have sufficient *in situ*  $^{10}$ Be to explain the high concentrations we measured in the non-quartz mineral phases.

Our results show that even small percentages of non-quartz mineral phases can have an appreciable effect on measured cosmogenic nuclide concentrations through the addition of meteoric  $^{10}$ Be and other impurities. Analyses of CRONUS-N without density separation (mean  $2.34 \times 10^5$  atoms  $g^{-1}$ , PRIME only) over-estimate the  $^{10}$ Be concentration by about 11% in relation to the material after performing density separation (mean  $2.11 \times 10^5$  atoms  $g^{-1}$ , PRIME only).

This offset would bias exposure ages too old or erosion rates too slow. However, the effect of non-quartz mineral phases varies randomly in CRONUS-N due to the small proportion and/or variable composition of non-quartz grains, as evidenced by the dispersion of <sup>10</sup>Be concentrations in relation to AMS counting statistics and the large spread in <sup>27</sup>Al and Mg concentrations.

Overall, we conclude that a small number of non-quartz grains, containing large concentrations of <sup>27</sup>Al, <sup>10</sup>Be, and impurities such as Mg, significantly influence measured cosmogenic nuclide concentrations in CRONUS-N.

#### 7.3. CRONUS-N Impurity and Reproducibility

Repeated analyses of CRONUS-N material demonstrate that sample impurity (and thus sample inhomogeneity) controls analytical reproducibility (Fig. 4). For CRONUS-N, we find that <sup>10</sup>Be analyses (n = 73) reproduced to 6.3%; this is about twice as large as the analytic uncertainty for the <sup>10</sup>Be measurements we report here (mean 3.1%, Table 1). Although the number of samples is considerably smaller, the CRONUS-N measurements made on material following density separation have an RSD of 3.2%, which is similar to the analytic uncertainty. For <sup>26</sup>Al, our data suggest that analyses reproduced to 7.7%, again similar to AMS counting statistics (Table 1). Overall, we show that aliquots of CRONUS-N that have been additionally treated and cleaned of all non-quartz mineral phases replicate better (and close to the total AMS error) than we document for untreated CRONUS-N material.

#### 7.4. Comparisons with a Liquid Reference Material

Unlike CRONUS-N, which is heterogeneous and appears to introduce dispersion beyond AMS analytical error, analyses of a homogeneous liquid reference material have less dispersion.

We compare our results for CRONUS-N to preliminary analyses of UVM-A (Corbett et al., 2019), which is dissolved CRONUS-A quartz (Jull et al., 2015) spiked with  $^9$ Be and  $^{27}$ Al to remove the variability of different stable isotope carriers between different preparation laboratories. The first 11 analyses of UVM-A at PRIME record a mean  $^{10}$ Be/ $^9$ Be ratio of (1.48 ± 0.07) x  $^{10^{-13}}$  (1SD), yielding an RSD of 4.6%. The mean analytic uncertainty of these measurements was (3.7 ± 0.6) %, yielding a dispersion of 1.2. For CRONUS-N, which is heterogeneous for  $^{10}$ Be, the same population size of 11 samples analyzed at the same AMS yielded an RSD of 5.8% and a dispersion of 1.7.

We surmise that solid (granular) and liquid reference materials test the reproducibility of different aspects of the laboratory process. If homogeneous, a granular reference material provides insight about stable isotope carrier concentration. A pre-spiked liquid reference material like UVM-A (Corbett et al., 2019) omits carrier variations and provides insight about batch-to-batch variability and AMS performance. However, an inhomogeneous granular reference material is not able to do any of the above successfully.

#### 8. Conclusions and Implications

After four years of analyses of the CRONUS-N reference material, numerous lines of evidence demonstrate that it is heterogeneous in regards to  $^{10}$ Be,  $^{27}$ Al, and impurities such as Mg. This heterogeneity is likely due to the presence of non-quartz mineral phases such as tourmaline, rutile, and spinel, which contain 22 times more  $^{10}$ Be than the purified quartz. Our analyses, which are over-dispersed for  $^{10}$ Be due to this heterogeneity, suggest replication to  $\sim$ 6%.

This work underscores the importance of thoroughly removing all non-quartz mineral phases from samples prepared for cosmogenic nuclide analysis. Our findings demonstrate that

non-quartz phases have the potential to contain over an order of magnitude more <sup>10</sup>Be than quartz. Even small masses of non-quartz grains in a sample can have an appreciable impact on measured concentrations because meteoric <sup>10</sup>Be appears to be retained in these dense and more chemically reactive mineral phases. Leaching in strong hydrochloric acid is insufficient to completely remove meteoric <sup>10</sup>Be from deep within fractures or alteration features in non-quartz mineral phases. Instead, complete removal of all non-quartz phases from a sample is the best way to maximize accuracy and reproducibility of samples.

#### Acknowledgements

AMS analysis of reference standards was supported by the Australian Nuclear Science and Technology Organization (ANSTO), Lawrence Livermore National Laboratory (LLNL), Purdue Rare Isotope Measurement (PRIME) Laboratory, and Scottish Universities Environmental Research Centre (SUERC). Corbett's time was supported by National Science Foundation EAR-1735676. We thank D. West and W. Amidon for assisting with SEM observations. Prepared in part by LLNL under Contract DE-AC52-07NA27344.; LLNL-JRNL-827885. We thank two anonymous reviewers and Editor P-H Blard for improving this manuscript with thoughtful comments.

#### References

- Auer, M., Kutschera, W., Priller, A., Wagenbach, D., Wallner, A., Wild, E., 2007. Measurement of <sup>26</sup>Al for atmospheric and climate research and the potential of <sup>26</sup>Al/<sup>10</sup>Be ratios. Nuclear Instruments and Methods in Physics Research Section B: Beam Interactions with Materials and Atoms 259, 595-599.
- Balco, G., 2011. Contributions and unrealized potential contributions of cosmogenic-nuclide exposure dating to glacier chronology, 1990-2010. Quaternary Science Reviews 30, 3-27.
- Balco, G., DeJong, B., Ridge, J., Bierman, P., Rood, D., 2021. Atmospherically-produced beryllium-10 in annually laminated late-glacial sediments of the North American Varve Chronology. Geochronology 3, 1-33.
- Balco, G., Rovey, C., 2008. An isochron method for cosmogenic-nuclide dating of buried soils and sediments. American Journal of Science 308, 1083-1114.
- Balco, G., Rovey, C., 2010. Absolute chronology for major Pleistocene advances of the Laurentide Ice Sheet. Geology 38, 795-798.
- Barg, E., Lal, D., Pavich, M., Caffee, M., Southon, J., 1997. Beryllium geochemistry in soils: evaluation of <sup>10</sup>Be/<sup>9</sup>Be ratios in authigenic minerals as a basis for age models. Chemical Geology 140, 237-258.
- Bender, A., Lease, R., Corbett, L., Bierman, P., Caffee, M., Rittenour, T., 2020. Late Cenozoic climate change paces landscape adjustments to Yukon River capture. Nature Geoscience 13, 571-575.
- Bierman, P., Caffee, M., 2002. Cosmogenic exposure and erosion history of Australian bedrock landforms. Bulletin of the Geological Society of America 114, 787-803.
- Bierman, P., Gillespie, A., Caffee, M., 1995. Cosmogenic ages for earthquake recurrence intervals and debris flow fan deposition, Owens Valley, California. Science 270, 447-450.
- Bierman, P., Nichols, K., 2004. Rock to sediment- slope to sea with <sup>10</sup>Be- rates of landscape change. Annual Review of Earth and Planetary Sciences 32, 215-255.
- Bierman, P., Steig, E., 1996. Estimating rates of denudation using cosmogenic isotope abundances in sediment. Earth Surface Processes and Landforms 21, 125-139.
- Bierman, P.R., Marsella, K.A., Patterson, C., Davis, P.T., Caffee, M., 1999. Mid-Pleistocene cosmogenic minimum-age limits for pre-Wisconsinan glacial surfaces in southwestern Minnesota and southern Baffin Island: a multiple nuclide approach. Geomorphology 27, 25-39.
- Binnie, S., Dewald, A., Heinze, S., Voronina, E., Hein, A., Wittmann, H., von Blanckenburg, F., Hetzel, R., Christl, M., Schaller, M., Leanni, L., Team, A., Hippe, K., Vockenhuber, C., Ivy-Ochs, S., Maden, C., Fulop, R.H., Fink, D., Wilcken, K., Fujioka, T., Fabel, D., Freeman, S., Xu, S., Fifield, L., Akcar, N., Spiegel, C., Dunai, T., 2019. Preliminary results of CoQtz-N: A quartz reference material for terrestrial insitu cosmogenic <sup>10</sup>Be and <sup>26</sup>Al measurements. Nuclear Instruments and Methods Section B: Beam Interactions with Materials and Atoms 456, 203-212.
- Blard, P.-H., Lupker, M., Rousseau, M., 2019. Paired-cosmogenic nuclide paleoaltimetry. Earth and Planetary Science Letters 515, 271-282.
- Brown, E., Bourlès, D., Raisbeck, G., Yiou, F., Burchfiel, B., Molnar, P., Qidong, D., Jun, L., 1998. Estimation of slip rates in the southern Tien Shan using cosmic ray exposure dates of abandoned alluvial fans. Geological Society of America Bulletin 110, 377-386.

- Brown, E., Edmond, J., Raisbeck, G., Yiou, F., Kurz, M., Brook, E., 1991. Examination of surface exposure ages of Antarctic moraines using in situ produced <sup>10</sup>Be and <sup>26</sup>Al. Geochimica et Cosmochimica Acta 55, 2269-2283.
- Brown, E., Stallard, R., Larsen, M., Raisbeck, G., Yiou, F., 1995. Denudation rates determined from the accumulation of in situ-produced <sup>10</sup>Be in the Luquillo Experimental Forest, Puerto Rico. Earth and Planetary Science Letters 129, 193-202.
- Caffee, M., Granger, D., Woodruff, T., 2015. The Gas-Filled-Magnet at PRIME Lab: Increased Sensitivity of Cosmogenic Nuclide Measurements. American Geophysical Union Fall Meeting Abstract ID V31G-09.
- Codilean, A., Fulop, R., Munack, H., Wilcken, K., Cohen, T., Rood, D., Fink, D., Bartley, R., Croke, J., Fifield, K., 2021. Controls on denudation along the East Australian continental margin. Earth-Science Reviews 214, 103543.
- Corbett, L., Bierman, P., Rood, D., Caffee, M., Lifton, N., Woodruff, T., 2017. Cosmogenic <sup>26</sup>Al/<sup>10</sup>Be Surface Production Ratio in Greenland. Geophysical Research Letters 44, 1350-1359.
- Corbett, L., Bierman, P., Woodruff, T., Caffee, M., 2019. A homogeneous liquid reference material for monitoring the quality and reproducibility of in situ cosmogenic <sup>10</sup>Be and <sup>26</sup>Al analyses. Nuclear Instruments and Methods Section B: Beam Interactions with Materials and Atoms 456, 180-185.
- Corbett, L.B., Bierman, P.R., Rood, D.H., 2016. An approach for optimizing in situ cosmogenic <sup>10</sup>Be sample preparation. Quaternary Geochronology 33, 24-34.
- Fabel, D., Harbor, J., 1999. The use of in-situ produced cosmogenic radionuclides in glaciology and glacial geomorphology. Annals of Glaciology 28, 103-110.
- Fink, D., Smith, A., 2007. An inter-comparison of <sup>10</sup>Be and <sup>26</sup>Al AMS reference standards and the <sup>10</sup>Be half-life. Nuclear Instruments and Methods in Physics Research Section B: Beam Interactions with Materials and Atoms 259, 600-609.
- Fujioka, T., Fink, D., Mifsud, C., 2015. Towards improvement of aluminium assay in quartz for in situ cosmogenic <sup>26</sup>Al analysis at ANSTO. Nuclear Instruments and Methods in Physics Research Section B: Beam Interactions with Materials and Atoms 361, 346-353.
- Gibbon, R., Pickering, T., Sutton, M., Heaton, J., Kuman, K., Clarke, R., Brain, C., Granger, D., 2014. Cosmogenic nuclide burial dating of hominin-bearing Pleistocene cave deposits at Swartkrans, South Africa. Quaternary Geochronology 24, 10-15.
- Gosse, J.C., Phillips, F.M., 2001. Terrestrial in situ cosmogenic nuclides: theory and application. Quaternary Science Reviews 20, 1475-1560.
- Graly, J., Bierman, P., Reusser, L., Pavich, M., 2010. Meteoric <sup>10</sup>Be in soil profiles A global meta-analysis. Geochimica et Cosmochimica Acta 74, 6814-6829.
- Granger, D., 2014. Cosmogenic nuclide burial dating in archaeology and paleoanthropology, In: Holland, H., Turekian, K. (Eds.), Treatise on Geochemistry. Elsevier, pp. 81-97.
- Granger, D., Caffee, M., Woodruff, T., 2014. A tenfold increase in <sup>26</sup>Al currents at PRIME Lab: Revisiting old ideas and exploring new possibilities with a gas-filled magnet. Geological Society of America Abstracts with Programs 46.
- Granger, D., Kirchner, J., Finkel, R., 1996. Spatially averaged long-term erosion rates measured from in situ-produced cosmogenic nuclides in alluvial sediment. The Journal of Geology 104, 249-257.
- Granger, D., Lifton, N., Willenbring, J., 2013. A cosmic trip: 25 years of cosmogenic nuclides in geology. Geological Society of America Bulletin 125, 1379-1402.

- Granger, D.E., Muzikar, P.F., 2001. Dating sediment burial with in situ-produced cosmogenic nuclides: theory, techniques, and limitations. Earth and Planetary Science Letters 188, 269-281.
- Hidy, A., Gosse, J., Sanborn, P., Froese, D., 2018. Age-erosion constraints on an Early Pleistocene paleosol in Yukon, Canada, with profiles of <sup>10</sup>Be and <sup>26</sup>Al: Evidence for a significant loess cover effect on cosmogenic nuclide production rates. Catena 165, 260-271.
- Hunt, A., Larsen, J., Bierman, P., Petrucci, G., 2008. Investigation of factors that affect the sensitivity of accelerator mass spectrometry for cosmogenic <sup>10</sup>Be and <sup>26</sup>Al isotope analysis. Analytical Chemistry 80, 1656-1663.
- Hunt, A., Petrucci, G., Bierman, P., Finkel, R., 2006. Metal matrices to optimize ion beam currents for accelerator mass spectrometry. Nuclear Instruments and Methods in Physics Research Section B: Beam Interactions with Materials and Atoms 243, 216-222.
- Hunt, A., Petrucci, G., Bierman, P., Finkel, R., 2007. Investigation of metal matrix systems for cosmogenic <sup>26</sup>Al analysis by accelerator mass spectrometry. Nuclear Instruments and Methods in Physics Research B 260, 633-636.
- Ivy-Ochs, S., Kubik, P., Masarik, J., Wieler, R., Bruno, L., Schlüchter, C., 1998. Preliminary results on the use of pyroxene for <sup>10</sup>Be surface exposure dating. Schweizerische Mineralogische und Petrographische Mitteilungen 78, 375-382.
- Jull, A., Scott, E., Bierman, P., 2015. The CRONUS-Earth inter-comparison for cosmogenic isotope analysis. Quaternary Geochronology 26, 3-10.
- Kohl, C.P., Nishiizumi, K., 1992. Chemical isolation of quartz for measurement of in-situ-produced cosmogenic nuclides. Geochimica et Cosmochimica Acta 56, 3583-3587.
- Leya, I., Michel, R., 2011. Cross sections for neutron-induced reactions up to 1.6 GeV for target elements relevant for cosmochemical, geochemical, and technological applications. Nuclear Instruments and Methods Section B: Beam Interactions with Materials and Atoms 269, 2487-2503.
- Matmon, A., Schwartz, D., Finkel, R., Clemmens, S., Hanks, T., 2005. Dating offset fans along the Mojave section of the San Andreas fault using cosmogenic <sup>26</sup>Al and <sup>10</sup>Be Geological Society of America Bulletin 117, 795-807.
- Merchel, S., Arnold, M., Aumaître, G., Benedetti, L., Bourlès, D., Braucher, R., Alfimov, V., Freeman, S., Steier, P., Wallner, A., 2008. Towards more precise <sup>10</sup>Be and <sup>36</sup>Cl data from measurements at the 10<sup>-14</sup> level: Influence of sample preparation. Nuclear Instruments and Methods in Physics Research Section B: Beam Interactions with Materials and Atoms 266, 4921-4926.
- Merchel, S., Bremser, W., Akhmadaliev, S., Arnold, M., Aumaître, G., Bourlès, D., Braucher, R., Caffee, M., Christl, M., Fifield, K., Finkel, R., Freeman, S., Ruiz-Gomez, A., Kubik, P., Martschini, M., Rood, D., Tims, S., Wallner, A., Wilcken, K., Xu, S., 2012. Quality assurance in accelerator mass spectrometry: Results from an international round-robin exercise for <sup>10</sup>Be. Nuclear Instruments and Methods Section B: Beam Interactions with Materials and Atoms 289, 68-73.
- Merchel, S., Gärtner, A., Beutner, S., Bookhagen, B., Chabilan, A., 2019. Attempts to understand potential deficiencies in chemical procedures for AMS: Cleaning and dissolving quartz for <sup>10</sup>Be and <sup>26</sup>Al analysis. Nuclear Instruments and Methods in Physics Research Section B: Beam Interactions with Materials and Atoms 455, 293-299.

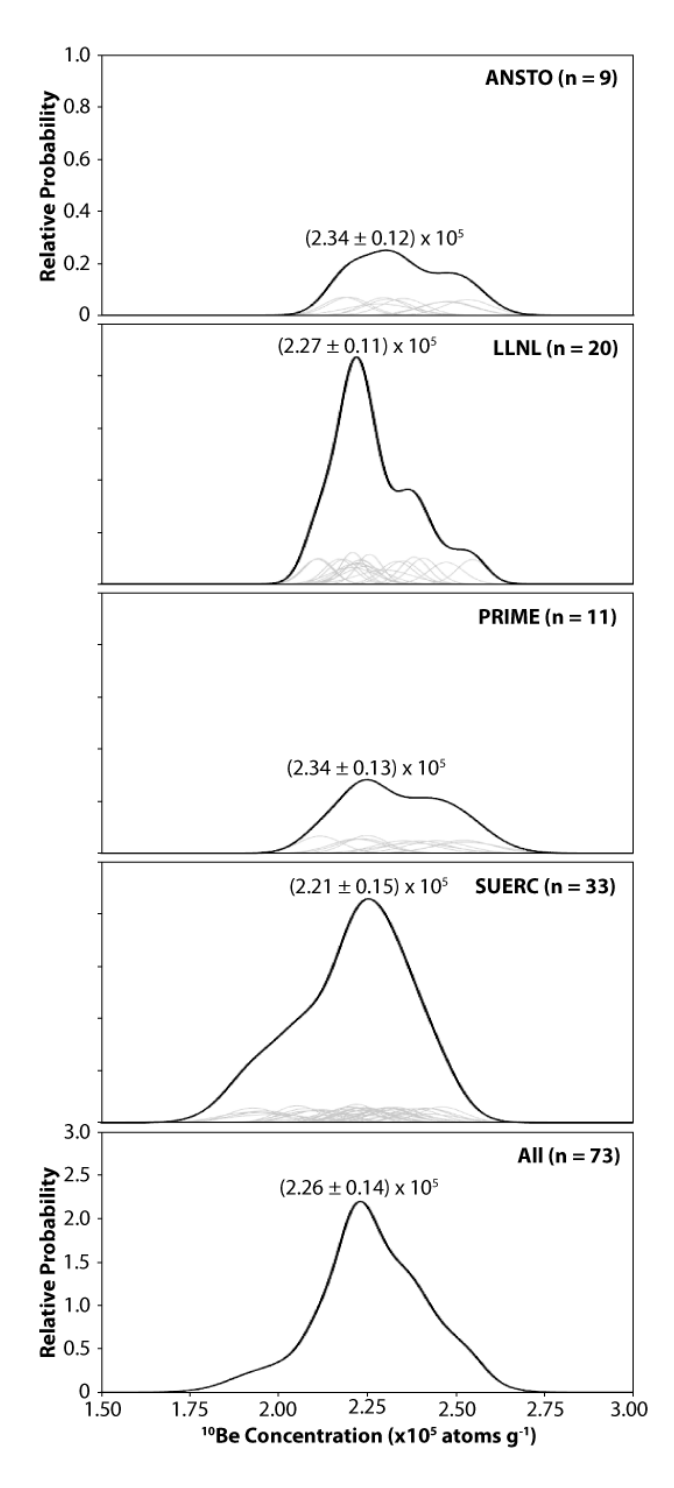
- Muzikar, P., Elmore, D., Granger, D., 2003. Accelerator mass spectrometry in geologic research. Geological Society of America Bulletin 115, 643-654.
- Nishiizumi, K., 2004. Preparation of <sup>26</sup>Al AMS standards. Nuclear Instruments and Methods in Physics Research Section B: Beam Interactions with Materials and Atoms 223-224, 388-392.
- Nishiizumi, K., Imamura, M., Caffee, M.W., Southon, J.R., Finkel, R.C., McAninch, J., 2007. Absolute calibration of <sup>10</sup>Be AMS standards. Nuclear Instruments and Methods in Physics Research Section B: Beam Interactions with Materials and Atoms 258, 403-413.
- Nishiizumi, K., Kohl, C., Arnold, J., Klein, J., Fink, D., Middleton, R., 1991. Cosmic ray produced <sup>10</sup>Be and <sup>26</sup>Al in Antarctic rocks: exposure and erosion history. Earth and Planetary Science Letters 104, 440-454.
- Nishiizumi, K., Kohl, C.P., Arnold, J.R., Dorn, R., Klein, I., Fink, D., Middleton, R., Lal, D., 1993. Role of in situ cosmogenic nuclides <sup>10</sup>Be and <sup>26</sup>Al in the study of diverse geomorphic processes. Earth Surface Processes and Landforms 18, 407-425.
- Nishiizumi, K., Lal, D., Klein, J., Middleton, R., Arnold, J., 1986. Production of <sup>10</sup>Be and <sup>26</sup>Al by cosmic rays in terrestrial quartz in situ and implications for erosion rates. Nature 319, 134-136.
- Phillips, F., Argento, D., Balco, G., Caffee, M., Clem, J., Dunai, T., Finkel, R., Goehring, B., Gosse, J., Hudson, A., Jull, A., Kelly, M., Kurz, M., Lal, D., Lifton, N., Marrero, S., Nishiizumi, K., Reedy, R., Schaefer, J., Stone, J., Swanson, T., Zreda, M., 2016. The CRONUS-Earth project: a synthesis. Quaternary Geochronology 31, 119-154.
- Portenga, E., Bierman, P., 2011. Understanding Earth's eroding surface with <sup>10</sup>Be. GSA Today 21, 4-10.
- Rood, D., Brown, T., Finkel, R., Guilderson, T., 2013. Poisson and non-Poisson uncertainty estimations of <sup>10</sup>Be/<sup>9</sup>Be measurements at LLNL-CAMS. Nuclear Instruments and Methods in Physics Research B 294, 426-429.
- Rood, D., Hall, S., Guilderson, T., Finkel, R., Brown, T., 2010. Challenges and opportunities in high-precision Be-10 measurements at CAMS. Nuclear Instruments and Methods in Physics Research Section B: Beam Interactions with Materials and Atoms 268, 730-732.
- Rood, D., Xu, S., Shank, R., Dougans, A., Gallacher, P., Keefe, K., Miguens-Rodriguez, M., Bierman, P., Carlson, A., Freeman, S., 2014. Towards high precision and low ratio Be-10 measurements with the SUERC 5MV tandem: bigger isn't always better. The Thirteenth International Conference on Accelerator Mass Spectrometry Programme and Abstracts, 53.
- Ruszkiczay-Rüdiger, Z., Neuhuber, S., Braucher, R., Lachner, J., Steier, P., Wieser, A., Braun, M., 2021. Comparison and performance of two cosmogenic nuclide sample preparation procedures of in situ produced <sup>10</sup>Be and <sup>26</sup>Al. Journal of Radioanalytical and Nuclear Chemistry 329, 1523-1536.
- Schaefer, J., Codilean, A., Willenbring, J., Lu, Z., Keisling, B., Fülöp, R.-H., Val, P., 2022. Cosmogenic nuclide techniques. Nature Reviews Methods Primers 2, 1-22.
- Schnabel, C., Reinhardt, L., Barrows, T., Bishop, P., Davidson, A., Fifield, L., Freeman, S., Kim, J., Maden, C., Xu, S., 2007. Inter-comparison in <sup>10</sup>Be analysis starting from pre-purified quartz. Nuclear Instruments and Methods in Physics Research Section B: Beam Interactions with Materials and Atoms 259, 571-575.

- Shanks, R., Freeman, S., 2015. Sputter-pits casting to measure AMS sample consumption. Nuclear Instruments and Methods Section B: Beam Interactions with Materials and Atoms 361, 168-172.
- Tuniz, C., Bird, J., Fink, D., Herzog, G., 1998. Accelerator Mass Spectrometry: Ultrasensitive Analysis for Global Science. CRC Press, Boston.
- von Blanckenburg, F., 2005. The control mechanisms of erosion and weathering at basin scale from cosmogenic nuclides in river sediment. Earth and Planetary Science Letters 237, 462-479.
- von Blanckenburg, F., Willenbring, J., 2014. Cosmogenic nuclides: dates and rates of Earth-surface change. Elements 10, 341-346.
- Willenbring, J., von Blanckenburg, F., 2010. Meteoric cosmogenic Beryllium-10 adsorbed to river sediment and soil: Applications for Earth-surface dynamics. Earth-Science Reviews 98, 105-122.

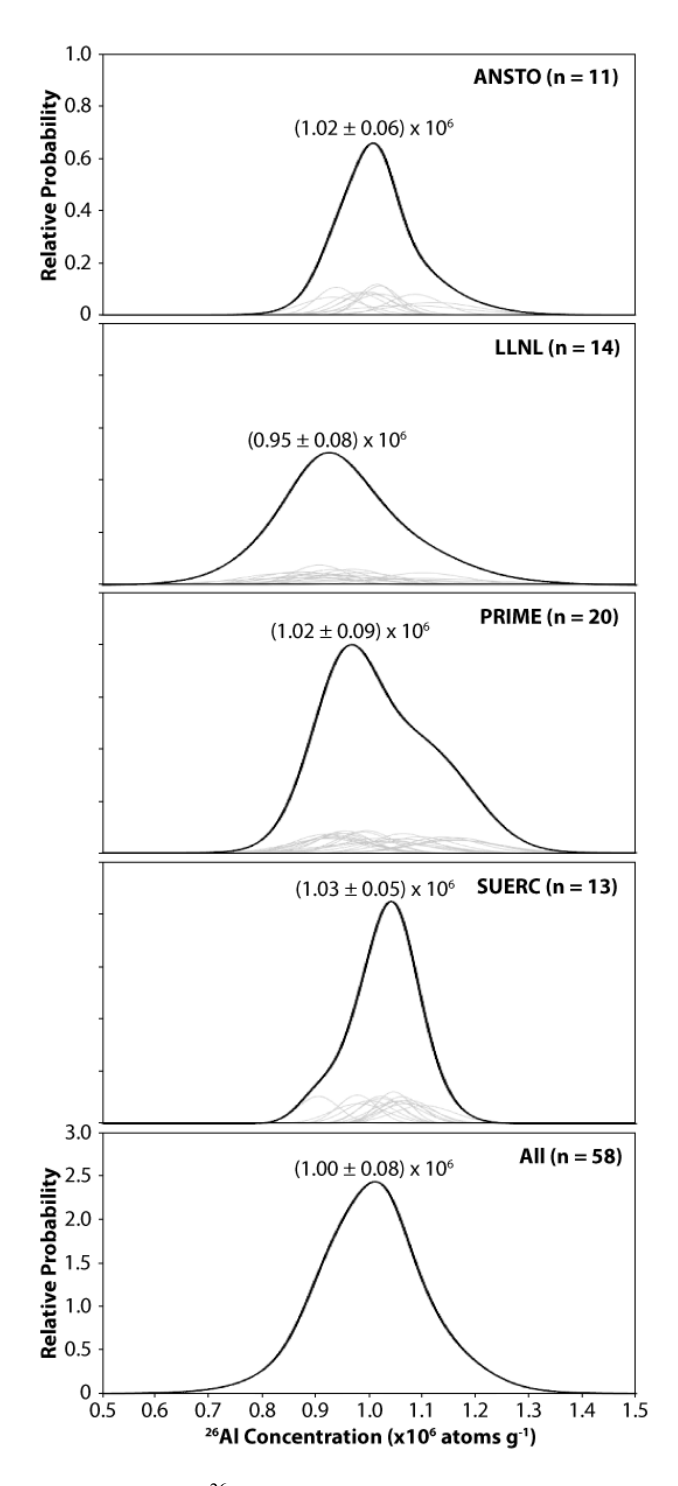
	<sup>10</sup> Be Data					<sup>26</sup> Al Data				
	Number of Analyses	<sup>10</sup> Be Concentration (x 10 <sup>5</sup> atoms g <sup>-1</sup> )	RSD of <sup>10</sup> Be Concentration (%)	Analytic Uncertainty (%)	Dispersion (RSD/Uncertainty)	Number of Analyses	<sup>26</sup> Al Concentration (x 10 <sup>6</sup> atoms g <sup>-1</sup> )	RSD of <sup>26</sup> Al Concentration (%)	Analytic Uncertainty (%)	Dispersion (RSD/Uncertainty)
ANSTO	9	2.34 +/- 0.12	5.3	2.9 +/- 0.5	1.8	11	1.02 +/- 0.06	5.7	5.3 +/- 2.0	1.1
LLNL	20	2.27 +/- 0.11	5.0	2.1 +/- 0.5	2.4	14	0.95 +/- 0.08	8.1	10.5 +/- 3.6	0.8
PRIME	11	2.34 +/- 0.13	5.8	3.4 +/- 0.4	1.7	20	1.02 +/- 0.09	8.4	6.5 +/- 1.3	1.3
SUERC	33	2.21 +/- 0.15	6.7	3.6 +/- 0.9	1.9	13	1.03 +/- 0.05	5.1	4.2 +/- 0.6	1.2
Overall	73	2.26 +/- 0.14	6.3	3.1 +/- 0.9	2.0	58	1.00 +/- 0.08	7.7	6.7 +/- 3.1	1.1
Jull et al. (2015)	23	2.17 +/- 0.09	4.1	3.5 +/- 2.4	1.2	10	1.05 +/- 0.11	10.1	8.4 +/- 4.4	1.2

Table 1.

**Table 1**.  $^{10}$ Be (n = 73) and  $^{26}$ Al (n = 58) concentrations of CRONUS-N reference material measured at four different AMS laboratories, as compared to data from Jull et al. (2015). The analystic uncertainty is calculated by averaging the individual errors for all samples analysed at each AMS lab. Sample preparation information can be found in Supplemental Data Table S1. Individual AMS measurements are detailed in Tables S2 and S3, with  $^{26}$ Al/ $^{10}$ Be ratios in Table S4. Blank data are in Tables S5 and S6.



**Figure 1**. Probability density functions of the <sup>10</sup>Be concentrations of CRONUS-N samples measured at each AMS laboratory. The top four plots for the four individual AMS laboratories have the same vertical scale; the bottom plot showing the compiled data has a different vertical scale due to the larger number of sample measurements. Thin gray lines show the central tendancy and uncertainty for each individual CRONUS-N sample, while thick black lines show the summed probability density function. The mean and one standard deviation are denoted above each summed central tendancy. Individual measurements are detailed in Supplemental Data Table S2.



**Figure 2**. Probability density functions of the <sup>26</sup>Al concentrations of CRONUS-N samples measured at each AMS laboratory. The top four plots for the four individual AMS laboratories have the same vertical scale; the bottom plot showing the compiled data has a different vertical scale due to the large number of sample measurements. Thin gray lines show the central tendancy and uncertainty for each individual measurement, while thick black lines show the summed probability density function. The mean and one standard deviation are denoted above each summed central tendancy. Individual measurements are detailed in Supplemental Data Table S3.

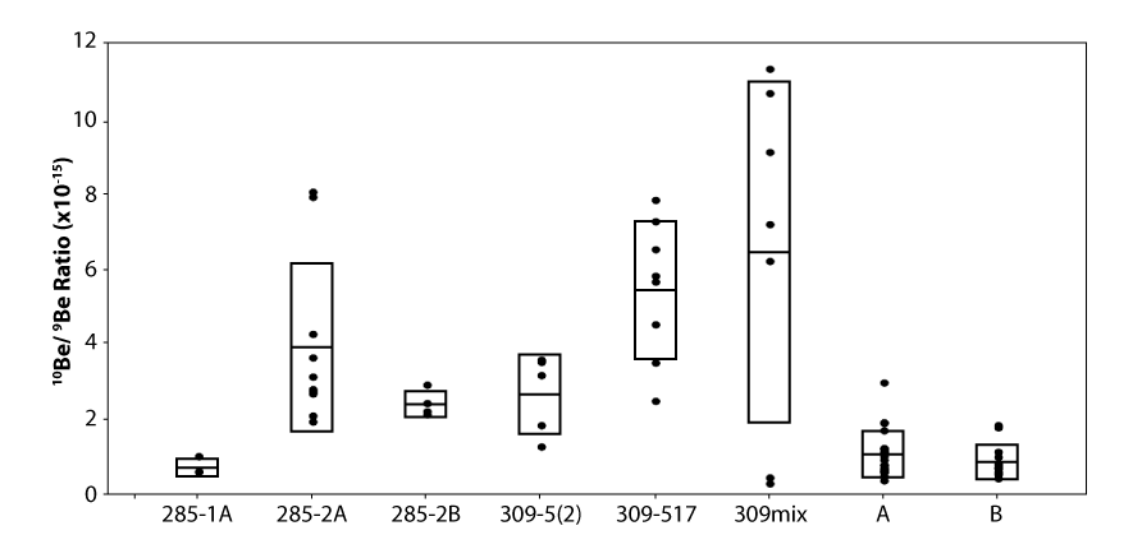


**Figure 3.** Measured blank ratios for eight different beryl carriers used over the study period. Carrier Be concentrations, which were quantified by ICP-OES, ranged from 291 to 449  $\mu$ g mL<sup>-1</sup>. For each process blank, we added sufficient volume of carrier to total ~250  $\mu$ g Be. Points show individual analyses ("285-1A" n = 3; "285-2A" n = 10; "285-2B" n = 4; "309-5(2)" n = 5; "309-517" n = 8; "309mix" n = 7; "A" n = 21; "B" n = 13). For each population of carrier measurements, rectangles show the measurement uncertainty, with the horizontal line denoting the mean; the upper and lower bounds of the rectangle denote  $\pm 1$  SD. Individual measurements are detailed in Supplemental Data Table S5.

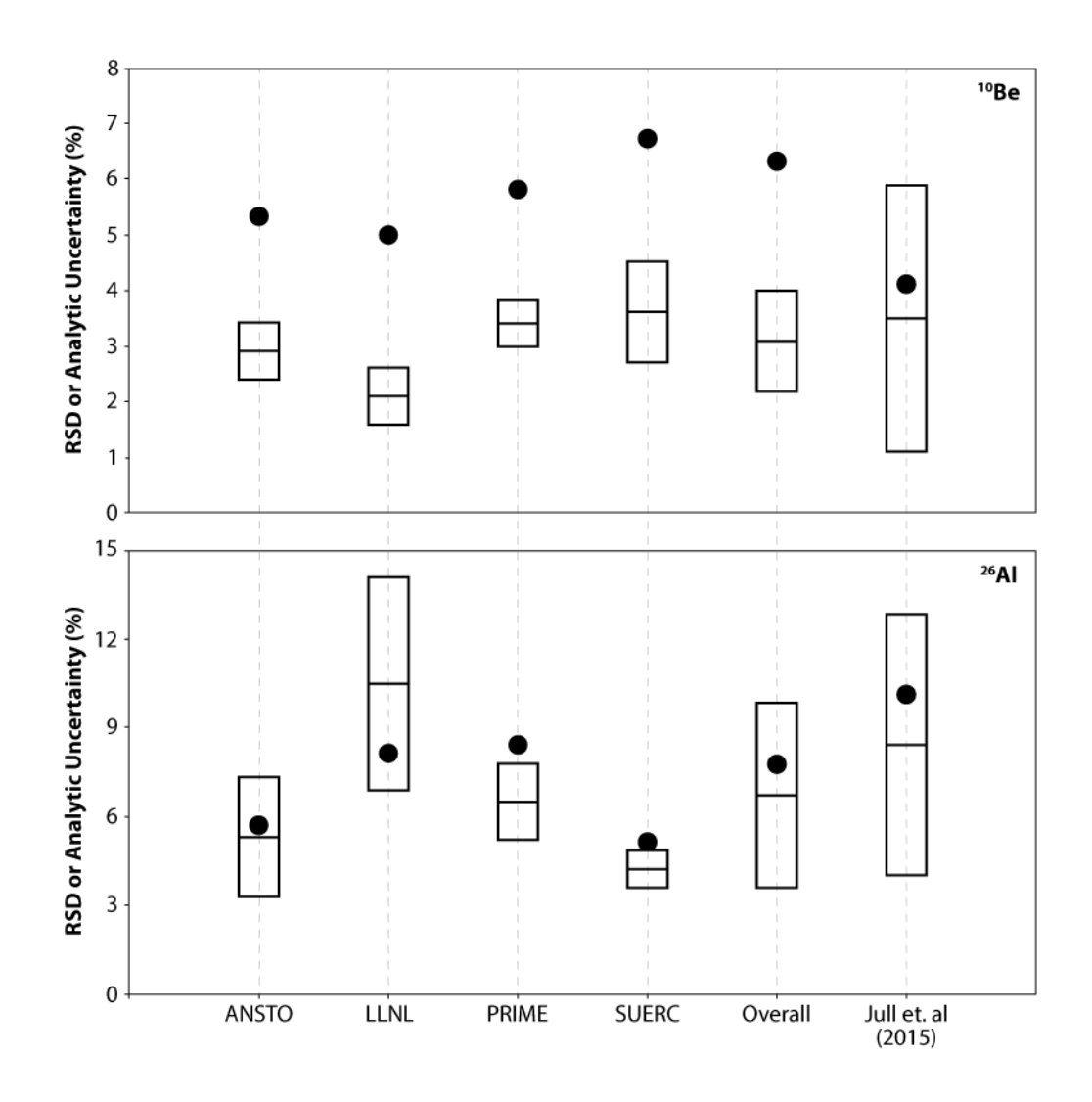


**Figure 4.** Depiction of the dispersion of AMS measurements for  $^{10}$ Be (top panel) and  $^{26}$ Al (bottom panel). Rectangles show the measurement uncertainty, with the horizontal line denoting the mean; the upper and lower bounds of the rectangle denote  $\pm 1$  SD. Black circles show the RSD of the calculated concentrations. Greater distance between the black circle and the rectangle shows greater dispersion. Note different vertical scales on the two plots due to the lower Poisson statistics for  $^{26}$ Al compared to  $^{10}$ Be. Individual measurements are detailed in Supplemental Data Tables S2 and S3, and summarized in Table 1.

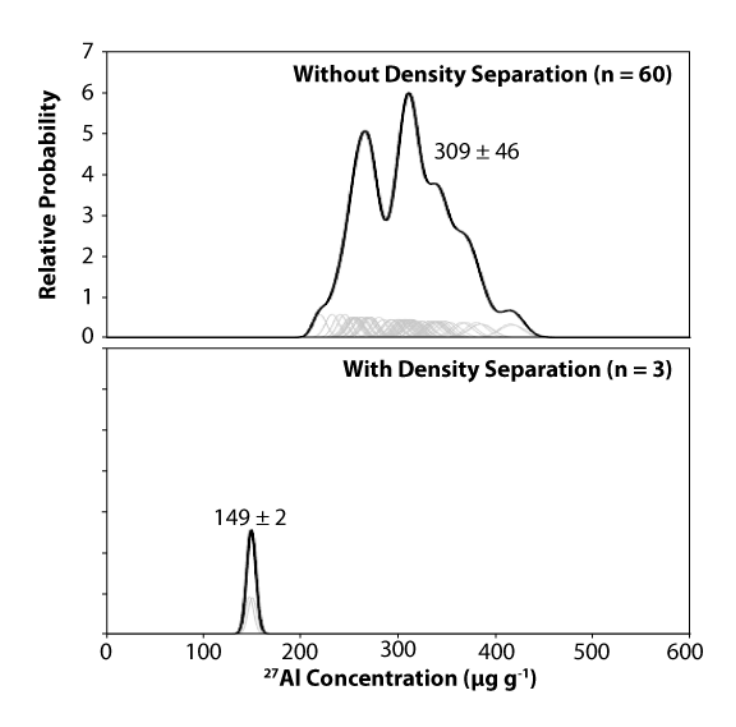


**Figure 5**. Probability density functions of stable <sup>27</sup>Al concentrations of CRONUS-N material without density separation (top panel) and after density separation (bottom panel). Concentrations were determined with ICP-OES. Both plots have the same vertical scale. Thin gray lines show the central tendancy and uncertainty for each individual measurement, while thick black lines show the summed probability density function. The mean and one standard deviation are denoted above each summed central tendancy.

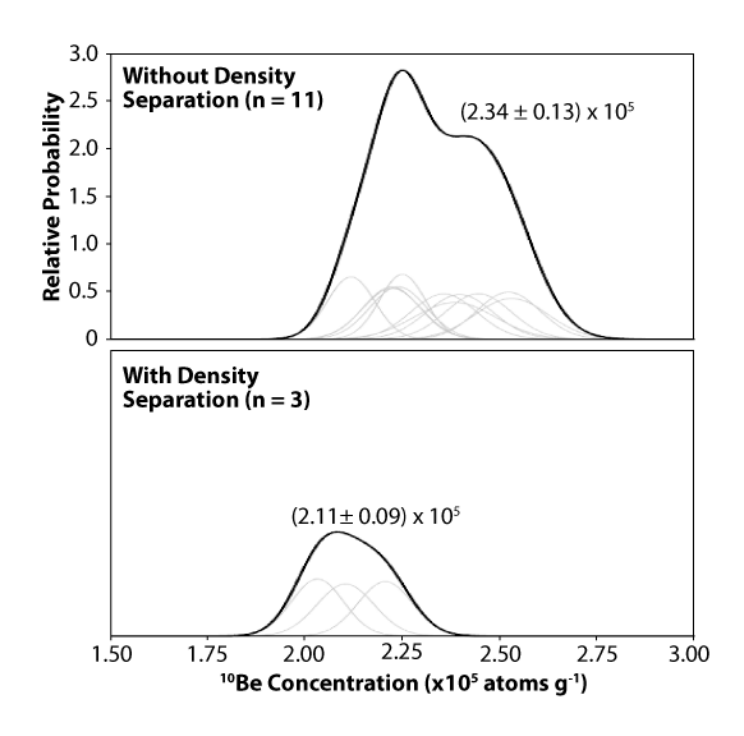


**Figure 6.** Probability density functions of <sup>10</sup>Be concentrations of CRONUS-N material measured at PRIME without density separation (top panel) and after density separation (bottom panel). Both plots have the same vertical scale. Thin gray lines show the central tendancy and uncertainty for each individual measurement, while thick black lines show the summed probability density function. The mean and one standard deviation are denoted above each summed central tendancy.

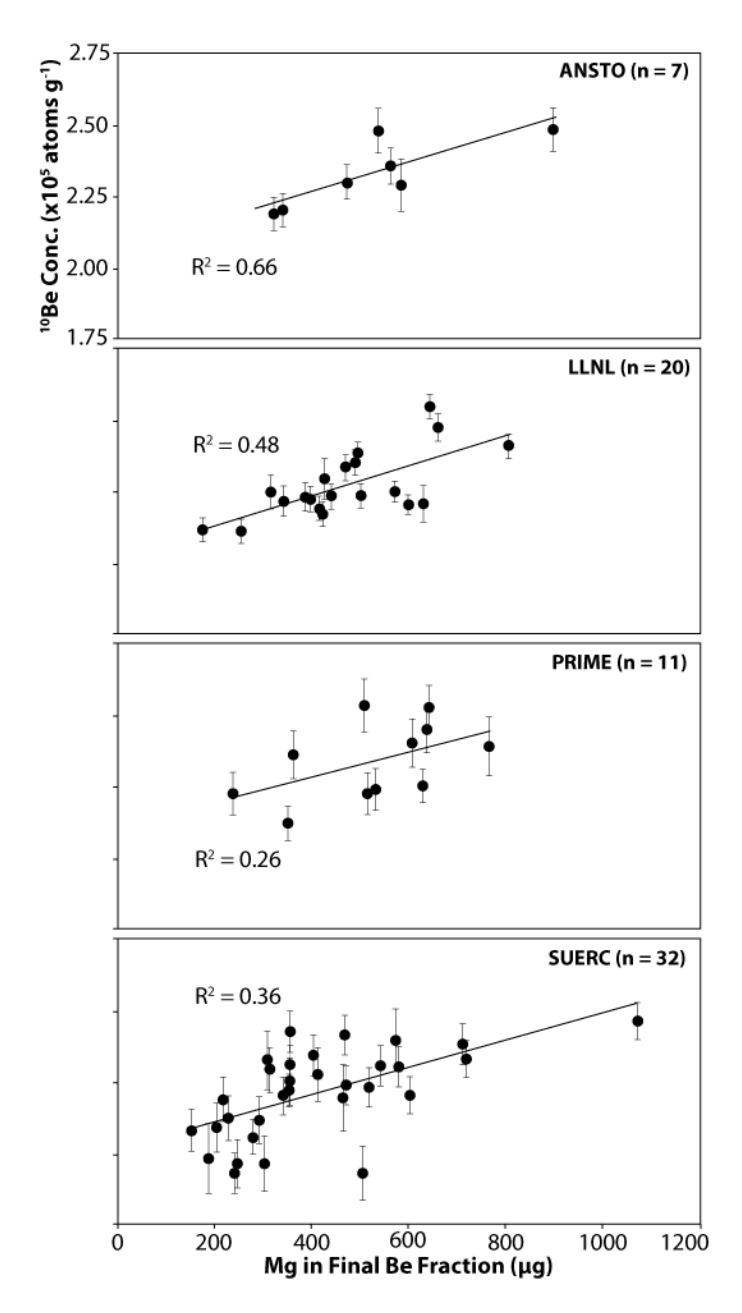


**Figure 7.** Linear regressions of calculated <sup>10</sup>Be concentration versus total Mg content at each AMS laboratory. All four plots have the same vertical scale. Error bars show 1σ uncertainties for individual <sup>10</sup>Be analyses. Mg contents in the final Be fractions were determined with ICP-OES purity testing upon completion of Be isolation but before gel precipitation; any Mg rejection during pH8 precipitation is not captured here. Note that two samples for ANSTO and one from SUERC have no Mg data due to ICP-OES failure. Individual measurements are detailed in Supplemental Data Table S2.

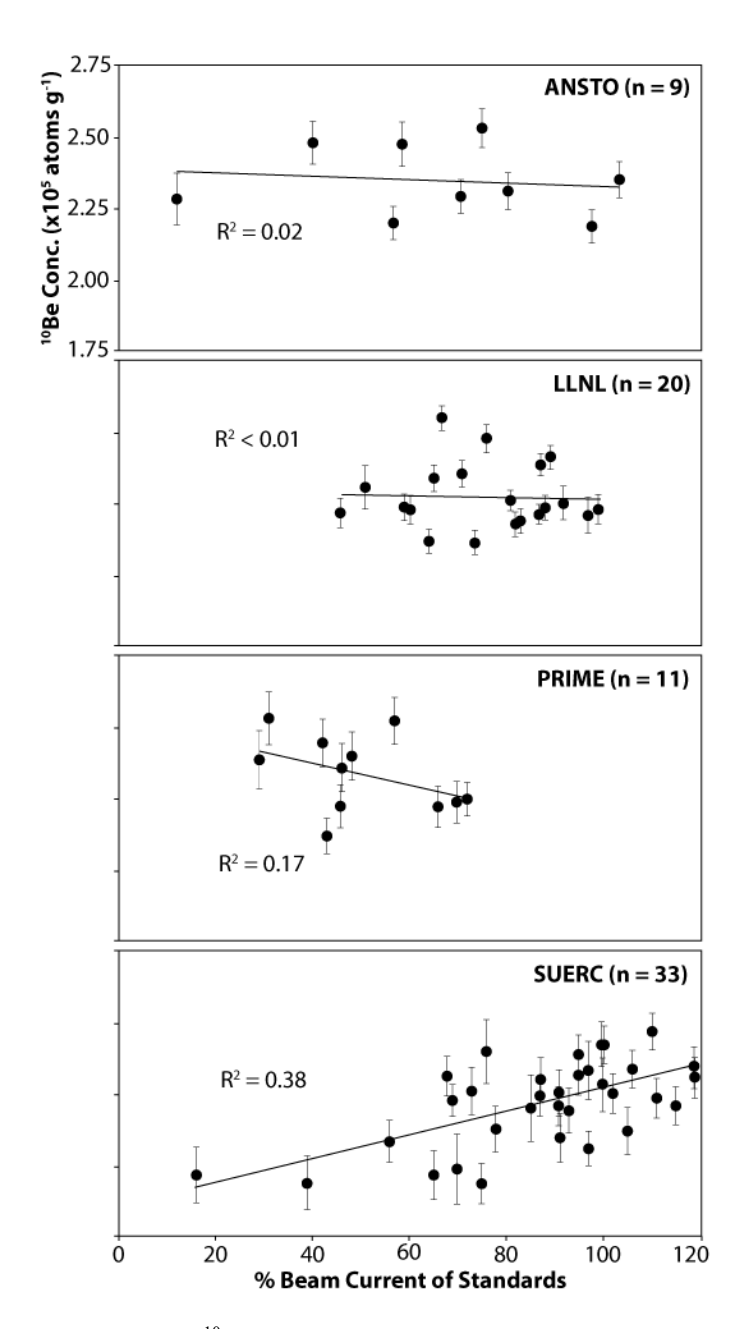


**Figure 8.** Linear regressions of calculated  $^{10}$ Be concentration versus normalized beam current at each AMS laboratory. All four plots have the same vertical scale. Error bars show  $1\sigma$  uncertainties for individual  $^{10}$ Be analyses. Sample beam currents were normalized to the beam currents of standards analyzed at the same time in order to account for variability in AMS performance; see text for details. Individual measurements are detailed in Supplemental Data Table S2.